State University, Stillwater, Okla. 74074.

[1]M. Mostoller, B. N. Ganguly, and R. F. Wood, Phys. Rev. B 4, 2015 (1971). An extensive list of references is contained in this paper.

[2]R. F. Blunt and M. I. Cohen, Phys. Rev. 153, 1031 (1967).

[3]O. E. Facey and W. A. Sibley, Phys. Rev. 186, 926 (1969); Phys. Rev. B 2, 1111 (1970).

[4]M. Mostoller, J. Phys. Chem. Solids (to be published).

[5]G. Gilat and L. J. Raubenheimer, Phys. Rev. 144, 390 (1966); L. J. Raubenheimer and G. Gilat, *ibid.* 157, 586 (1967).

[6]R. S. Katiyar, J. Phys. C 3, 1693 (1970).

[7]C. C. Klick, D. A. Patterson, and R. S. Knox, Phys. Rev. 133, A1717 (1964).

PHYSICAL REVIEW B VOLUME 4, NUMBER 8 15 OCTOBER 1971

Structure in the Neutron Scattering Spectra of Zirconium Hydride†

J. G. Couch*
Southern Oregon College, Ashland, Oregon 97520

and

O. K. Harling and Lavern C. Clune
Battelle Memorial Institute, Pacific Northwest Laboratory, Richland, Washington 99352

(Received 7 June 1971)

Neutron double-differential cross sections of four polycrystalline samples of ZrH_x with hydrogen-to-zirconium ratios (x) of 0.54, 1.03, 1.56, and 2.00 have been measured with high-energy resolution by downscattering of neutrons from initial energies of 171.5 and 244.8 meV. Clear evidence of structure in the one-phonon optical peak of ZrH_2 is observed for the first time. This structure consists of two maxima located at energy transfers of 137 and 143 meV and a shoulder located at 154 meV. Similar structure is indicated for the other hydride samples but it becomes less well defined as the hydrogen-to-zirconium ratio decreases. The observed structure is compared with predictions of a central-force model calculation by Slaggie, which includes the effects of interactions between hydrogen atoms. The widths of the hydrogen vibration peaks are found to depend upon the zirconium-to-hydrogen ratio as well as upon the momentum transferred in the scattering process.

I. INTRODUCTION

One reason zirconium hydride has attracted interest during the past few years is because the hydrogen atoms appear to behave somewhat as independent Einstein oscillators in the zirconium lattice. Neutron-scattering experiments[1-5] and heat-capactiy measurements[6,7] lend support to this simple model; both give consistent results indicating a vibration-level spacing of about 140 meV. Significant differences between experiment and the Einstein model do exist, however, and they have stimulated further efforts to understand the zirconium-hydrogen system in more detail. For one thing, the widths of the optical peaks obtained by neutron-scattering experiments indicate a much broader frequency distribution than that predicted by this theoretical single-frequency model, even with Doppler broadening and contributions from low-energy acoustic modes taken into account.[8,9]

At least two models—the Gaussian-plus-Debye (GD) model[9-11] and the central-force (CF) model[12]—have been used to account for the width of the first optical peak in ZrH_2. The GD phenomenological model uses a combination of an optical level with a Gaussian distribution of frequencies plus a Debye spectrum. The CF model extends the Einstein model by taking into account the longer-range forces, the H-H interactions in particular, in explaining the broad optical peak. An interesting feature of the CF model is its prediction of structure in the optical peak.

The various published zirconium-hydride neutron double-differential cross-section results[1-5] are generally consistent with an optical-peak location and width corresponding to the first vibration level of 140 meV and ~26 meV, respectively. However, none of these data reported in the literature reveal detailed shape or structure in the optical peaks. Although previous measurements have shown that the peak shape, particularly the width, does not change significantly with hydrogen concentration,[2,7,10,11,13,14] one might expect that any finer structural characteristics of the scattering peaks will differ noticeably for different H/Zr ratios.

In the present work we report high-resolution neutron-downscattering measurements of polycrystalline zirconium hydride, carried out at two different incident energies (171.5 and 244.8 meV) and four different hydrogen concentrations ($ZrH_{0.54}$,

$ZrH_{1.03}$, $ZrH_{1.56}$, and $ZrH_{2.00}$). Structure in the one-phonon optical peak is observed for all concentrations studied, the structure for $ZrH_{2.00}$ being the most evident. A comparison is made between the experimental double-differential cross sections for $ZrH_{2.00}$ and the prediction of the CF model.

II. EXPERIMENTAL DETAILS

Details of the Battelle rotating-crystal spectrometer used in this work have been described elsewhere.[15] In all, eight data sets were collected, four at each of two different incident neutron energies. Table I summarizes the experimental energy resolutions used in the measurements reported here. Flight paths (fp) of 1.5 m were used in all cases except for 16° at 244.8 meV, where a 4.0-m fp was used. All data were collected at a room temperature of ~296 °K.

The incident energy of 244.8 meV was chosen because it yields inelastically scattered neutrons of sufficiently high energy to ensure minimal multiple scattering, as predicted by total-cross-section curves,[16] and yet it is low enough that only one optical phonon can be excited. The 4.0-m fp was used at 16° for this incident energy in order to improve the experimental resolution because resolutions are relatively large for a 1.5-m fp at this high energy. A lower incident neutron energy of 171.5 meV was also used to obtain favorable resolutions even though the very low energy of neutrons scattered inelastically at this incident energy has a much higher cross section for multiplte scattering.[2]

Measurements made using an empty target assembly were used to correct for background in the experiments done at 244.8 meV and also for the $ZrH_{1.56}$ and $ZrH_{1.03}$ experiments done at 171.5 meV. Background corrections for the other 171.5-meV data were made by simply subtracting a constant background determined from the extremes of the time-of-flight spectrum. This is justified because the background measurements gave only a flat structureless spectrum in the region of the inelastic peak.

TABLE I. The incident neutron energies E_1 are given with energy spread due to Bragg uncertainty only. The total resolution on downscattered neutrons for an energy transfer of 140 meV is also tabulated as ΔE and includes all appropriate resolution elements.

$E_1 = 171.5 \pm 3.4$ meV		$E_1 = 244.8 \pm 3.5$ meV	
θ_s (deg)	ΔE (meV)	θ_s (deg)	ΔE (meV)
14.5	4.1	16	5.0
29.6	4.2	29.6	9.0
44.5	4.3	44.5	10.0
59.5	4.5	59.5	11.2
90.5	5.0	90.5	13.9
121	4.2	119.5	8.9
		156	11.8

TABLE II. ZrH_x target properties.

x	at.%	Crystal phase	Thickness (g/cm^2)	Percent transmission
0.54	35.1	$\alpha+\delta+\gamma$	0.87	84.4
1.03	50.8	$\alpha+\delta+\gamma$	0.47	86.8
1.56	60.9	$\delta+\gamma$[a]	0.24	90.4
2.00	66.7	ϵ	0.24	88.8

[a]Reference 6 shows samples at this hydrogen concentration to be ~97% δ phase. Reference 17 gives ~93% δ phase, ~7% γ phase.

The four targets used in this work consisted of commercially available ZrH_x powder samples sandwiched between two 7.6×15.2×0.025-cm aluminum sheets. Basic properties of the targets are summarized in Table II. The hydrogen contents listed in Table II were determined by a method of driving off hydrogen from known weights of the

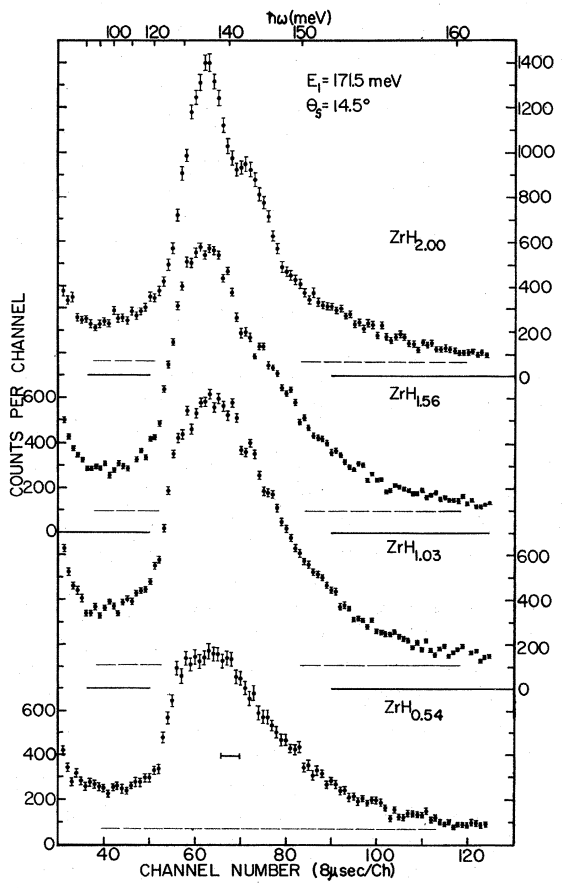

FIG. 1. Typical time-of-flight spectra of neutrons scattered by $ZrH_{0.54}$, $ZrH_{1.03}$, $ZrH_{1.56}$, and $ZrH_{2.00}$ at an incident energy of 171.5 meV. Only data in the region of the optical peak are shown. The dashed lines indicate approximate background levels.

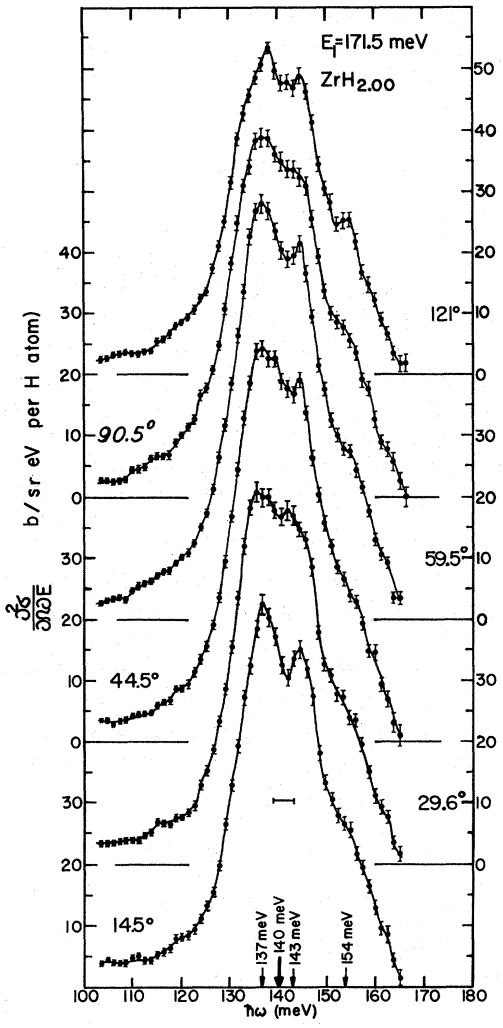

FIG. 2. Double-differential cross sections for neutrons scattered by $ZrH_{2.00}$ at an incident energy of 171.5 meV. Only results in the region of the optical peak are shown. The small arrows at the bottom of the figure indicate the locations of fine structure and the large arrow indicates the center of the main peak.

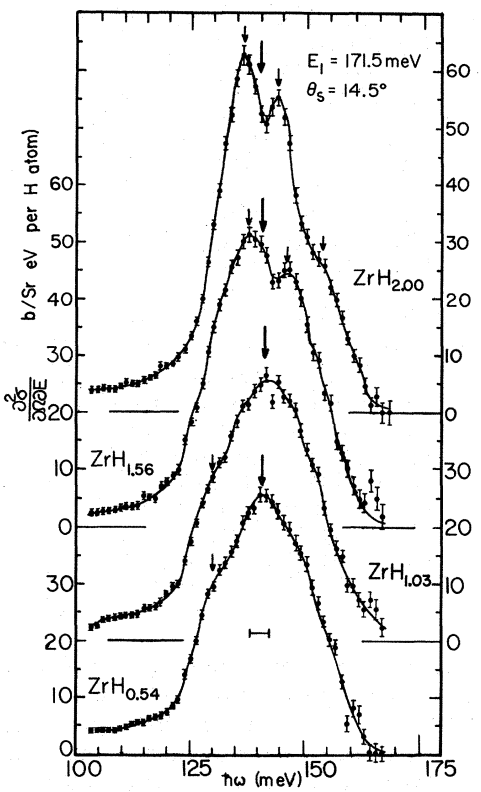

FIG. 3. Typical double-differential cross sections for neutrons scattered by $ZrH_{0.54}$, $ZrH_{1.03}$, $ZrH_{1.56}$, and $ZrH_{2.00}$ at an incident energy of 171.5 meV and a scattering angle of 14.5°. Large arrows indicate centers of the inelastic peak and small arrows indicate the location of any structure in the peak. Only results in the region of the optical peak are shown.

powder, in a furnace, and measuring the gas pressure developed in a known volume. Hydrogen contents quoted by the manufacturer are in good agreement with the tabulated values.

III. EXPERIMENTAL RESULTS

Typical time-of-flight (TOF) spectra in the region of the inelastic peak are shown in Fig. 1 for the 171.5-meV data sets. The experimental resolution in the region of the combined elastic and acoustic phonon peak, which would be centered at about channel 24 in Fig. 1, was too coarse to allow examination of the peak shape in any detail. Furthermore, comparable data for the quasi-elastic peak have already been published.[4,5] Consequently, results of measurements in the neighborhood of the elastic peak are not included in this study. The dashed lines in Fig. 1 represent approximate back-

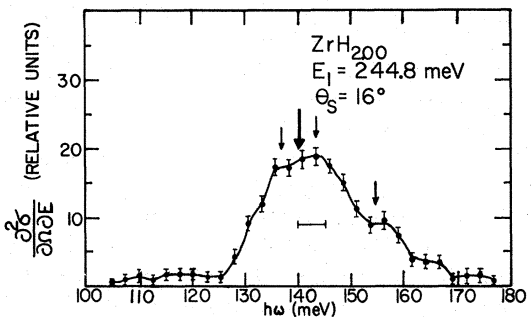

FIG. 4. Double-differential cross section for neutrons scattered by $ZrH_{2.00}$ at 16° with an incident energy of 244.8 meV. The small arrows indicate the location of structure and the large arrow the center of the main peak for neutrons scattered at 14.5° by $ZrH_{2.00}$ at an incident energy of 171.5 meV.

TABLE III. Peak locations $\hbar\omega$ (meV) for ZrH_x for incident energies E_1 and scattering angles θ_s.

θ_s \ x	0.54	1.03	1.56	2.00	
		$E_1 = 244.8$ meV			
16°	143.6	143.4	142.3	142.5	
29.6°	142.8	142.8	142.3	141.8	
44.5°	142.8	143.1	141.5	141.5	
59.5°	143.1	143.6	142.0	142.0	
90.5°	144.1	144.6	142.8	143.1	
119.5°	145.1	146.1	144.8	144.8	
156°	147.6	146.9	143.1	144.1	
av	144.2	144.4	142.7	142.8	143.5 ± 0.3
		$E_1 = 171.5$ meV			
14.5°	140.5	141.0	140.6	140.0	
29.6°	140.5	140.6	140.4	139.9	
44.5°	140.4	140.4	139.9	139.7	
59.5°	140.0	140.8	140.0	139.7	
90.5°	140.4	140.2	140.2	139.7	
121°	141.0	141.4	141.1	140.3	
av	140.5	140.7	140.4	139.9	140.4 ± 0.1

ground levels. The horizontal bar centered at the peak location represents the spectrometer resolution. This resolution is calculated from all known elements, including the energy spread and time width of the incident neutrons, and the elements due to various path-length uncertainties.[15] The resolution is represented in a similar manner in the cross-section curves that follow. Error bars in the TOF data and in the cross sections are due to counting statistics only.

The raw TOF data have been converted by computer to double-differential cross sections per hydrogen atom, with normalizations using assumed cross sections for zirconium and hydrogen of 6.2 and 22.3 b, respectively. Representative double-differential cross sections are shown in Figs. 2–4. These cross sections are plotted against energy transfer $\hbar\omega = E_1 - E_2$, where E_1 and E_2 are the initial and scattered neutron energies, respectively. The large arrows in the figures indicate the center of the inelastic peak [determined by bisecting a line drawn full width at the half-maximum (FWHM)] and the shorter arrows indicate the location of any structure in the peak.

The locations of the center of the one-phonon optical peak at all scattering angles for the eight different data sets are listed in Table III. Average peak locations for the 244.8- and 171.5-meV measurements are 143.5 ± 0.3 and 140.4 ± 0.1 meV, respectively. The uncertainties represent random errors only and are expressed as deviations from the mean in each case. Estimates of possible systematic errors are 1.0 and 0.7 meV for the 244.8- and 171.5-meV data, respectively.

FWHM values of the optical peak corrected for experimental resolution are displayed in Fig. 5.

A scale of momentum transfer κ, rather than scattering angle θ_s, was chosen so that widths obtained at the two different incident energies could be compared directly. κ and θ_s are related by

$$\kappa = \frac{(2m)^{1/2}}{\hbar} \left[E_1 + E_2 - 2(E_1 E_2)^{1/2} \cos\theta_s\right]^{1/2},$$

where m is the neutron mass, $\hbar$ is Planck's constant, and E_1 and E_2 are the initial and scattered neutron energies, respectively. Typical estimated errors for the FWHM values, representative of all the peaks at 244.8 meV, are shown only for $ZrH_{2.00}$. FWHM values for the 171.5-meV peaks could be determined with considerably more certainty because of the smaller statistical errors involved; estimated errors for these peak widths are represented approximately by the sizes of the symbols.

IV. DISCUSSION OF RESULTS

Locations and widths of the optical peak appear to depend on incident energy as shown in Table III and Fig. 5. Some of the observed differences may be due to systematic errors arising from the different operating conditions at the two incident energies. However, even small differences in peak shape, possibly due to different amounts of multi-

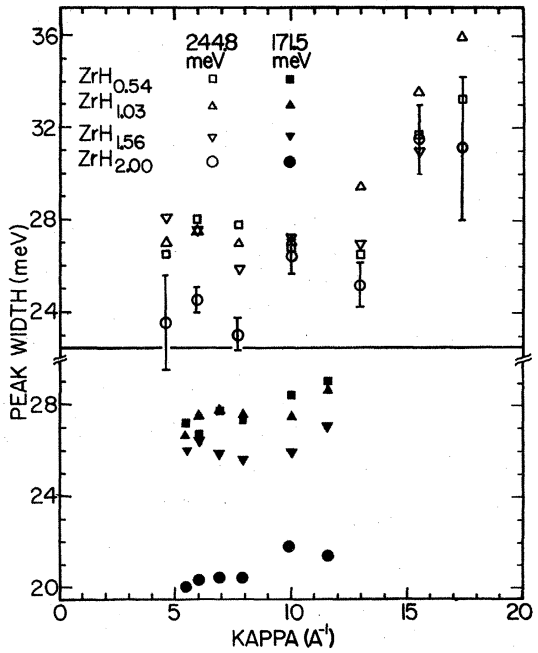

FIG. 5. Width (FWHM) of the inelastic double-differential cross-section peak in energy units vs momentum transfer for different H/Zr ratios. Error bars represent typical uncertainties in 244.8-meV widths (open symbols). Errors for 171.5-meV widths (filled symbols) are typically the size of the symbol. Widths have been corrected for experimental resolution.

phonon contributions at these two energies, have a noticeable influence on the measured peak locations and widths. For example, compare the shapes of the $ZrH_{2.00}$ peak at $E_1 = 244.8$ meV (Fig. 4) to the same peak at $E_1 = 171.5$ meV (Fig. 2). The half-height positions of the 171.5-meV peaks lie slightly above the shoulder on the right side of the peak, whereas the half-height position falls slightly below the shoulder on the 244.8-meV peak. This tends to give a greater measured width and a slightly higher measured value for the location of the peak centers for 244.8-meV initial energy.

An increase in peak width with momentum transfer is indicated by the results shown in Fig. 5. Both multiphonon scattering and multiple scattering of neutrons are expected to make small contributions to the width. The amount of multiphonon scattering increases monotonically with momentum transfer, whereas multiple scattering effects are expected to be at a minimum at 45° and 135° scattering angles because the 45° orientation of the target with respect to the incident neutrons gives a minimum effective target thickness for second scattering at these angles. The observed variation with scattering angle indicates that multiphonon scattering is the major cause of the increase in width.

A variation in peak width with hydrogen concentration is apparent in Fig. 5, in contrast to several previous reports that widths are independent of concentration for ZrH_x.[2,7,10,11,14] At 171.5-meV incident energy the peak widths for $ZrH_{2.00}$ are substantially less, about 20%, than those for the other hydrogen concentrations, and the widths for $ZrH_{1.56}$ somewhat less than those for $ZrH_{0.54}$ and $ZrH_{1.03}$. At 244.8 meV the differences in peak widths for the various concentrations are less dramatic. Peak widths at this energy for targets of $H/Zr < 2.00$ are approximately the same regardless of hydrogen concentration, but the $ZrH_{2.00}$ widths tend to be consistently lower than the widths for the other sample concentrations in the region of small κ. The similarity of peak width for $ZrH_{1.0}$ and $ZrH_{0.54}$ at both initial energies is in contrast to an earlier report[13] that the peak width continued to increase with decreasing hydrogen concentration in this region.

Inspection of the cross sections of Fig. 2, for $ZrH_{2.00}$ at various scattering angles, reveals structure in the inelastic scattering peaks. There are two maxima near the center of the optical peak at about 137 and 143 meV as well as a shoulder at 145 meV. This is believed to be the first clear experimental evidence for structure of this type in zirconium hydride or any other metal hydride. The energy locations of the fine structure and also the center of the peak are approximately the same for all scattering angles and are indicated by the small arrows and large arrow, respectively, at the bottom of the figure. Some smoothing of the structure is observed as the scattering angle is increased.

Figure 3 presents the small-angle scattering cross sections for all the hydride samples. These results indicate that structure in the optical peak decreases with hydrogen concentration. The cross section for $ZrH_{1.56}$ is similar to that for $ZrH_{2.00}$ although the two maxima near the center are slightly broadened and shifted to higher energy, and there is no clear evidence for a shoulder near 154 meV. For the $ZrH_{1.03}$ data shown in Fig. 3, any indication of structure near the center of the peak or for a shoulder at 154 meV can be attributed to statistical scatter in the data. However, the results for $ZrH_{1.03}$ at other scattering angles (not shown) do give persistent evidence for separate maxima at approximately 140 and 145 meV, the structure being comparable to error limits, but no clear evidence for a shoulder at 154 meV. Data with improved statistics would clear up the question of structure near the center of the $ZrH_{1.03}$ peaks. There is a shoulder at ~130 meV in the cross-section peaks for $H/Zr = 0.54$ and 1.03 which is not seen in the higher hydrides. For the $ZrH_{0.54}$ data there is no evidence of structure near the center of the band, or for a shoulder at 154 meV.

The fine structure near the center of the optical peak generally becomes less distinct as the scattering angle is increased. This can be seen in Fig. 2 for ZrH_2, but the same trend is observed in the results for the other hydrides. This progressive smoothing probably reflects the increase in multiphonon scattering mentioned earlier, and is evidence that the fine structure itself is not caused by either multiphonon excitation or multiple scattering of neutrons.

The structure in the $ZrH_{2.00}$ data for 244.8 meV incident energy and 16° scattering angle, shown in Fig. 4, is not as well defined as in the corresponding 171.5-meV data. This is probably due to the shorter counting times with resultant poorer statistics. The arrows in Fig. 4 indicate the location of structure found in the 171.5-meV data. There are some indications of similar structure in the 244.8-meV data. The cross sections for the other hydrides and scattering angles obtained with 244.8-meV incident energy are not shown since the poorer energy resolution at angles other than 16° (see Table I) would not allow positive identification of fine structure.

Slaggie[12] has carried out the lattice-dynamical calculation for ZrH_2, assuming CF, in an attempt to relate the shape of the frequency distribution to the interatomic forces. After making the simplification that ZrH_2 is fcc [ZrH_2 is actually fct with $c/a = 0.89$], he introduced four force constants, each related to one of the interactions: Zr–Zr,

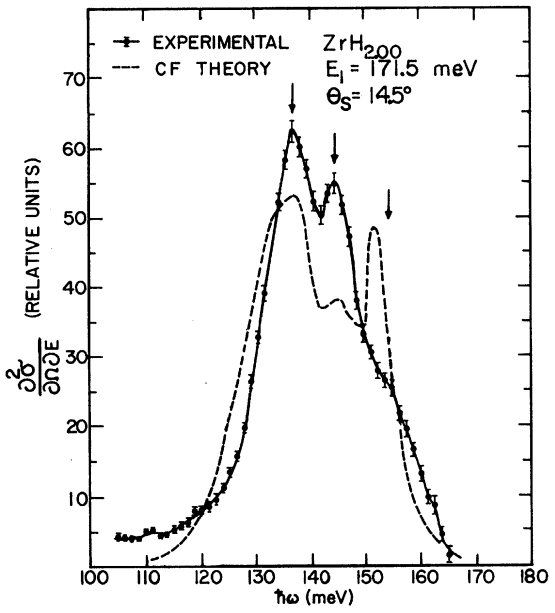

FIG. 6. Comparison of CF theory for the optical scattering peak with experimental results for 171.5-meV incident energy. The CF-model curve has been shifted by approximately 3 meV to allow for the difference between optical-peak energy used in the theory and the experimental position of the center of the main vibration peak. No other normalizations or shifts were applied to the theoretical or experimental results. Arrows represent the locations of the fine structure in the experimental data.

Zr–H (nearest neighbors), H-H (second nearest neighbors), and H-H (third nearest neighbors). The Zr-Zr force is related to acoustic modes, the Zr-H nearest-neighbor force determines the position of the optical frequencies, and the H-H forces cause a splitting of the optical peak. A frequency spectrum and corresponding double-differential cross-section curve were reported by Slaggie[12] for a representative incident energy (239 meV), scattering angle (40°), optical-peak position (137 meV), and width (20 meV). (Spacial averaging was included to allow for polycrystalline materials.)

The CF-model–calculated double-differential cross-section curve is reproduced in Fig. 6 together with experimental results for comparison, even though the conditions for the theoretical calculation and the experimental cross section do not match precisely. The energy scale of the CF curve was shifted by 3 meV to account for differences between theory and experiment in peak position. No cross-section normalizations have been made. The CF curve appears to have three maxima. The most dominant maxima at the highest and lowest energies are attributed to second-nearest-neighbor hydrogen interactions and the much smaller maximum near the center arises from third-nearest-neighbor hydrogen interactions.

The cross-section results for both ZrH_2 and $ZrH_{1.56}$ (Figs. 3 and 6) have two maxima that are qualitatively similar to the two most dominant maxima of the CF-model calculation. The dominant maxima of the CF curve have a larger energy separation than the experimental maxima but improved agreement would be attained by choosing a smaller second-nearest-neighbor H-H interaction in the CF-model calculation. Although Slaggie's choice for the strength of the second-nearest-neighbor H-H interactions does predict structure at approximately 154 meV, as indicated in Fig. 6, the shoulder observed at this energy in the cross sections for ZrH_2 is qualitatively different and is assumed to be due to other effects. The lack of evidence for structure at 154 meV in the results for $ZrH_{1.56}$, which is predominantly cubic δ phase, suggests that the shoulder may be due to the tetragonal structure of the ϵ-phase ZrH_2 which was not considered by Slaggie.

The deviation from cubic symmetry of the ZrH_2 lattice should be important in determining the shape of the optical peak. If CF interactions between the H atoms and the nearest Zr neighbors alone are considered, the localized hydrogen vibrations should correspond to two distinct frequencies. There should be a nondegenerate frequency (ω_1) corresponding to vibrations parallel to the c axis and a doubly degenerate frequency (ω_2) corresponding to vibrations in the plane perpendicular to the c axis. It can be shown that these frequencies are related to the c/a ratio of the fct lattice such that $\omega_2 = (a/c)\omega_1$. Therefore for ZrH_2, where $a/c = 1.12$, the hydrogen-vibration modes would be comprised of two different frequencies which are separated by 12% or approximately 17 meV. When interactions between hydrogen and its second and third nearest neighbors are considered, then only for the infinite-wavelength vibration modes in which the hydrogen atoms vibrate in phase and opposite the lattice of zirconium atoms should the above calculation provide a reasonable estimate of the splitting due to tetragonality. For finite wavelengths and for the vibration modes in which the fct hydrogen lattices vibrate against each other, interactions between hydrogen and its second and third nearest neighbors will be important, and result in a more complicated frequency distribution. It would be interesting to compare the measured cross sections for ZrH_2 with a refined lattice-dynamical calculation which incorporates the effects of tetragonality.

ACKNOWLEDGMENTS

The authors are indebted to Dr. W. D. McCormick for his assistance with some of the experiments in the early stages of this work. Ap-

preciation is also experssed to G. D. Seybold and Thomas Traver for their help in data reduction, and to Michael Linville for his assistance in preparing the graphs.

†Paper based on work performed under the U.S. AEC Contract No. AT(45-1)-1830 and was supported in part by the Battelle Memorial Institute.

*Faculty Appointee under appointment from the Northwest College and University Association for Science, Richland, Wash.

[1]I. Pelah, C. M. Eisenhauer, D. J. Hughes, and H. Palevsky, Phys. Rev. 108, 1091 (1957); A. Andresen, A. W. McReynolds, M. Nelkin, M. Rosenbluth, and W. Whittemore, *ibid.* 108, 1092 (1957).

[2]W. L. Whittemore, in *Proceedings of the Fourth Symposium on Inelastic Scattering of Neutrons in Solids and Liquids, Bombay*, (IAEA, Vienna, 1965), Vol. II, p. 305.

[3]A. D. B. Woods, B. N. Brockhouse, M. Sakamoto, and R. N. Sinclair, in *Proceedings of the First Symposium on Inelastic Scattering of Neutrons in Solids and Liquids, Vienna*, 1960 (IAEA, Vienna, 1961), p. 487.

[4]B. K. Harling and B. R. Leonard, Jr., BNL Report No. 940 (*C*-45), 1966, p. 96 (unpublished).

[5]S. N. Purohit, S. S. Pan, F. Bischoff, W. A. Bryant, C. Lajeunasse, M. L. Yeater, W. E. Moore, G. J. Kirvouc, L. J. Each. and N. C. Francis, in *IAEA Symposium on Neutron Thermalization and Reactor Spectra, Ann Arbor*, 1967 (IAEA, Vienna, 1968), p. 407.

[6]W. J. Tomasch, Phys. Rev. 123, 510 (1961).

[7]H. E. Flotow and D. W. Osborne, J. Chem. Phys. 34, 1418 (1961).

[8]D. H. Saunderson and S. J. Cocking, in *Proceedings of the Second Symposium on Inelastic Scattering of Neutrons in Solids and Liquids, Chalk River*, 1962 (IAEA, Vienna, 1963), Vol. II, p. 265.

[9]S. S. Pan, W. E. Moore, and M. L. Yeater, Trans. Am. Nucl. Soc. 9, 495 (1966).

[10]J. C. Young, J. A. Young, G. K. Houghton, G. D. Trimble, and J. R. Beyster, Nucl. Sci. Eng. 19, 230 (1964).

[11]J. W. Koppel, U.S. AEC Report No. GA-7055, 1966 (unpublished).

[12]E. L. Slaggie, J. Phys. Chem. Solids 29, 923 (1968).

[13]S. S. Pan, Ph.D. thesis (Rensselaer Polytechnic Institute, 1967) (unpublished).

[14]W. L. Whittemore, U.S. AEC Report No. GA-4990, 1964 (unpublished).

[15]O. K. Harling, Rev. Sci. Instr. 37, 697 (1966); in *Proceedings of the Fourth Symposium on Neutron Inelastic Scattering, Copenhagen* (IAEA, Vienna, 1968), Vol. II, p. 271.

[16]W. L. Whittemore and A. W. McReynolds, Phys. Rev. 113, 806 (1958).

[17]R. L. Beck, Trans. Am. Soc. Metals 55, 542 (1962).

PHYSICAL REVIEW B VOLUME 4, NUMBER 8 15 OCTOBER 1971

Diffusion of Helium Isotopes in Vitreous Silica*

J. E. Shelby
Sandia Laboratories, Livermore, California 94550

The diffusion of He^3 and He^4 in vitreous silica was experimentally measured in the temperature range 100–760 °C. The ratio of the diffusion coefficients is given by $D(He^3)/D(He^4) = (1.205 \pm 0.003) \exp[-(131 \pm 7 \text{ cal/g-at.})/RT]$. These results cannot be explained by classical diffusion theory, which does not predict an isotope effect in the activation energy for diffusion. The quantum corrections proposed by LeClaire for the special case of low-atomic-mass isotope diffusion satisfactorily explain the observed results.

I. INTRODUCTION

There have been several studies of the diffusion of He^4 in vitreous silica,[1–5] but only one determination of the relative diffusivities of He^3 and He^4 in vitreous silica has been reported.[6] Jones[6] calculated the isotopic diffusivity ratio from the corresponding ratios for permeability and solubility. However, no direct determination of the diffusivity of He^3 in glass has been previously reported.

The magnitude of the experimentally observed isotope effect, when compared with theoretically predicted values, should allow a distinction between various possible diffusion mechanisms. Classical diffusion theory predicts that the ratio of the isotopic diffusion coefficients should vary as the reciprocal of the square root of the mass of the diffusing atoms.[7] LeClaire[8] has suggested that a quantum correction be applied to classical theory when the diffusing species are of low atomic mass. He has applied these corrections to hydrogen isotope diffusion in metals with some success. However, this analysis has not been tested on helium isotope diffusion because of a lack of experimental data. The relatively large values of the He^4 diffusivity in vitreous silica[1–5] would suggest that a helium isotope diffusion study in this material might provide a significant test of LeClaire's the-